Electron and hole microwave cyclotron resonance in photoexcited undoped GaAs/$Al_{0.3}Ga_{0.7}As$ multiple quantum wells

M. Kozhevnikov,* E. Cohen, and Arza Ron
Solid State Institute, Technion–Israel Institute of Technology, Haifa 32000, Israel

Hadas Shtrikman
Department of Condensed Matter Physics, The Weizmann Institute of Science, Rehovot 76100, Israel
(Received 10 August 1999)

We studied the microwave cyclotron resonance (CR) of photoexcited free and weakly localized electrons and holes in undoped GaAs/$Al_{0.3}Ga_{0.7}As$ multiple quantum wells (MQW's) of various well widths. The photoinduced microwave absorption was measured at a frequency of $\omega_{mw}=35.6$ GHz and at various lattice temperatures in the range of $T_L=4.2-300$ K. The interband excitation intensity was very low, so that the density of photogenerated electrons and holes was of the order of $n\leqslant 10^8$ cm^{-2}. In all the studied QW's, an electron CR was observed, while a heavy hole CR was measured only in narrow QW's. By model fitting the CR line shape, the electron and hole cyclotron masses and the electron scattering rate dependence on T_L and on the microwave power were obtained. Assuming that the electron in-plane mobility at ω_{mw} is proportional to the inverse scattering rate, we find that it varies in the range of $(0.8-8)\times 10^5$ cm^{2}V^{-1} sec^{-1} for 100 Å and 200 Å MQW's. This is less than the mobility measured in modulation doped QW's of similar widths. We present a detailed analysis of the temperature dependence of the electron scattering rate by combining the electron-phonon, electron-impurity, and electron-interface roughness scattering rates. The latter is found to be an important scattering mechanism in undoped MQW's at low temperatures. The CR analysis also shows that the electron cyclotron mass varies (in the range of $0.055-0.070m_0$) with increasing either T_L or the microwave power. These variations are interpreted in terms of weak electron localization in large area, in-plane potential fluctuations arising from interface roughness. [S0163-1829(99)06547-9]

I. INTRODUCTION

Electron scattering processes in a two-dimensional (2D) semiconductor system were first studied in Si inversion layers.[1,2] Then, with the advent of improved growth techniques, modulation doped GaAs heterostructures[3] were shown to have a very high dc mobility of the two-dimensional electron gas (2DEG) at low lattice temperatures ($T_L<20$ K). In these quantum structures the charge carrier-impurity scattering is reduced by having a large spacer separating the dopants layer from the 2DEG or two-dimensional hole gas (2DHG), and by the screening of the random electrostatic potential fluctuations.[4,5]

Measuring the mobility of a very low density, photoexcited 2DEG (or 2DHG) in an undoped MQW is much more difficult than in the case of high densities in a modulation-doped heterostructure. One of the most powerful methods for the study of charge carrier scattering mechanisms in semiconductors is the cyclotron resonance (CR) technique.[6,7] So far, conventional CR has been studied in doped semiconductors,[8,9] while optically detected CR (ODCR) has been studied in both doped and undoped samples.[10,11] In most cases, CR is studied in the quantum limit,[8–11] where high magnetic fields and far infrared (FIR) radiation are used in order to overcome the large linewidth encountered in bulk and QW samples with relatively low mobility.

A CR study at microwave (mw) frequencies in III-V semiconductors requires low magnetic fields ($B\sim 1$ T), so that the energy separation $\hbar\omega_c$ between adjacent Landau levels is usually smaller than the thermal energy (k_BT_L).[12] This experimental condition is termed ''classical CR,'' as the carrier transport can be described by a classical equation of motion. On the other hand, the FIR CR usually requires $1<B<20$ T, and then the carrier Landau quantization is important (quantum limit). In the classical case, the line shape of the mw power absorption dependence on B, assuming a linearly polarized mw radiation having a frequency ω and an electric-field strength $E(\omega)$, is given by[13]

$$P(B)=\frac{ne^2\tau}{m^*}|E(\omega)|^2\frac{1+(\omega^2+\omega_c^2)\tau^2}{[1+(\omega^2-\omega_c^2)\tau^2]^2+4\omega_c^2\tau^2}. \quad (1)$$

Here, $\omega_c=eB/m^*$ is the cyclotron frequency, n, m^*, and τ are the density, effective mass, and momentum relaxation time (at microwave frequencies) of the charge carrier, respectively. Clearly, the required condition in order to observe a resonancelike CR trace as given by Eq. (1) is $\omega_c\tau\geqslant 1$. Consequently, only samples with very high carrier mobility satisfy this mw CR condition under low magnetic fields.[12,14]

The classical and quantum CR limits differ also in the relaxation times of the carriers. The classical CR relaxation time, τ, [deduced from Eq. (1)] is expected to be roughly equal to that deduced from dc conductivity measurements, as observed in high mobility GaAs/$Al_{0.3}Ga_{0.7}As$ heterojunctions with various electron concentrations.[14] The reason is that under mw CR conditions, the carriers are moving in large cyclotron orbits and then τ is mainly sensitive to back

 ©1999 The American Physical Society

scattering.[15] On the other hand, the relaxation time that is deduced from FIR CR line shape and from Shubnikov–de Haas measurements (namely, the ''quantum lifetime'' or the electronic eigenstate lifetime) is sensitive to scattering into all angles.[16]

We report on a mw CR study of very low density-free and weakly localized electrons and holes in photoexcited, undoped GaAs/$Al_{0.3}Ga_{0.7}As$ MQW's at various T_L in the range 4.2–300 K. The objectives of this paper are (i) to demonstrate the conditions under which the method of photoinduced microwave absorption (PMA) and its excitation (PMAE) spectroscopy is very useful for the detection of a very low density of photoexcited electrons and holes in QW's, and (ii) to analyze the mw CR line shape and from it to extract the temperature dependence of the electron relaxation time and (in-plane) cyclotron effective mass.

This paper shows that the electron relaxation time at mw frequency and at low temperatures is smaller in GaAs MQW's than that measured in bulk GaAs of the same quality. The experimental temperature dependence of the relaxation time is compared with the theoretically calculated scattering rates, using the models of electron-phonon, electron-impurity, and electron-interface roughness scattering processes. We then conclude that electron scattering by the spatially fluctuating QW interface potential is of major importance even in wide QW's. The analysis of the electron cyclotron mass dependence on the temperature and mw power indicates that it is subjected to weak in-plane localization that is probably due to large area interface islands.

This paper is laid out as follows: In Sec. II, the experimental setup, the samples used, and the experimental results are presented. An analysis of the experimental data and its discussion are given in Sec. III. Section IV concludes this paper. In the appendix, we compare some ODCR measurements with those observed by the conventional mw CR method.

II. EXPERIMENTAL PROCEDURE AND RESULTS

The undoped GaAs/$Al_{0.3}Ga_{0.7}$ As MQW's (of various well widths) were grown on (001)-oriented GaAs substrates by molecular beam epitaxy. Each sample consists of 25 wells with 200 Å wide $Al_{0.3}Ga_{0.7}As$ barriers. Detailed results are presented here for MQW's with well widths of $L_w = 50$, 100, and 200 Å. The sample was placed at the antinode of the mw electric field in an 8-mm waveguide that is short circuited by a plunger at one end. The mw radiation of 35.6 GHz reflected from the plunger was directed onto a diode detector by a circulator. The incident mw power, P_{mw}, was continuously varied by an electrically controlled attenuator so that the power incident on the sample was in the range of $P_{mw} = 0.1$–50 mW. The waveguide was immersed either in liquid He or in cold He gas, and the temperature was varied in the range of $T_L = 4.2$–300 K. The sample was illuminated by laser light (from a He-Ne or a tunable dye laser) through a pinhole in the waveguide. The light intensity I_L was sufficiently low so that the photogenerated free electron density was of the order of $n_e \leq 10^8\ cm^{-2}$ for $I_L \leq 10\ mW/cm^2$. The laser beam was modulated at a frequency varying in the range of $f_{mod} = 10$ Hz–1 MHz.

The mw radiation absorption by the MQW increases by the photoexcitation of unbound electrons and holes. The modulated mw radiation signal that is reflected from the plunger and is measured by the diode detector (and is proportional to the mw power absorbed by the photoexcited sample) is the measured PMA. The spectrum obtained by monitoring the PMA signal while scanning the photoexcitation energy is the PMAE spectrum (this spectrum is a counterpart of the PLE spectrum). For cyclotron resonance measurements, an external dc magnetic field **B** was applied parallel to the [001] direction and was swept over the range 0–1 T. The mw electric field was polarized perpendicularly to **B**, and the absorbed mw power was measured as a function of magnetic field intensity.

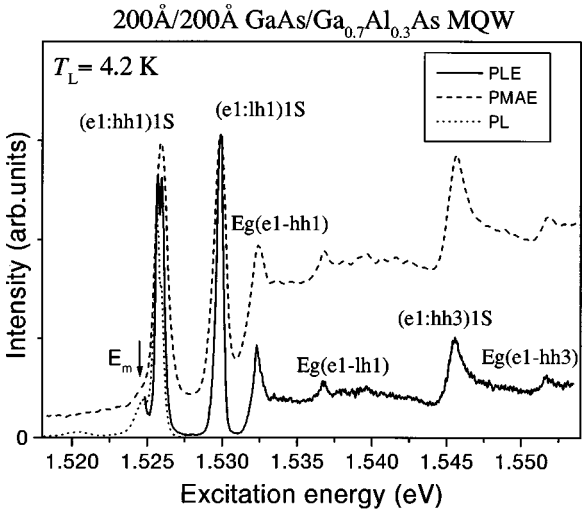

FIG. 1. The photoluminescence (PL) and its excitation (PLE) spectra observed with no microwave irradiation at $I_L = 100\ mW/cm^2$. The PLE spectrum is monitored at E_m. The photoinduced microwave absorption excitation (PMAE) spectrum was obtained at $P_{mw} = 5\ mW$ with photomodulation at $f_{mod} = 900$ Hz.

Figure 1 shows the PL, PLE, and PMAE spectra of the $L_w = 200$ Å MQW (measured at $B = 0$). Such spectra were measured for all the MQW structures studied here and are used in order to characterize them, by comparing the mw absorption with the interband optical transitions, as explained in Sec. III.

Figure 2 shows the PMA dependence on B observed for the 200 Å MQW for various T_L. Only an electron CR band is observed for this MQW, and its linewidth increases as T_L increases. Generally, the PMA signal may be due to free carriers that are excited in the QW's as well as in the GaAs buffer layer and substrate. We observed that the PMA intensity increases when the magnetic field satisfies the electron CR condition ($B \sim 0.09$ T at the mw frequency of 35.6 GHz), as shown in the inset of Fig. 2. Since this PMA increase occurs for photoexcitation in the QW spectral region only, we conclude that the CR signal is due only to electrons confined to the QW's.

A similar (but broader) electron CR band was observed in the 100 Å MQW. In addition to the electron CR band, this MQW shows another CR band with a resonance field, which is very sensitive to P_{mw}, as shown in Fig. 3. The analysis, given in the next section, indicates that this CR band is due to the QW's heavy holes (hh).

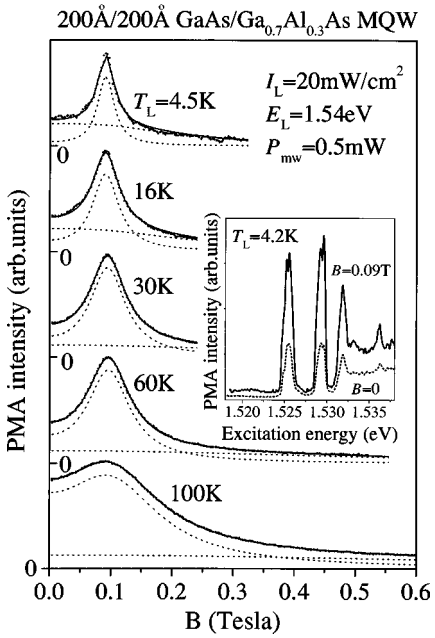

FIG. 2. The magnetic-field dependence of the photoinduced microwave absorption (PMA) measured at five different temperatures (solid curves). The deconvolution into an electron cyclotron resonance (CR) band originating from the MQW and a very broad CR band originating from the GaAs buffer layer and substrate [both calculated using Eq. (1)] are shown by dashed lines. Their sum is shown by the dotted line that virtually overlaps the experimental trace. The insert shows the PMAE spectra at $B=0$ and $B\sim 0.09$ T (magnetic-field strength of the electron CR).

The PMAE spectra of the 200 Å and 100 Å MQW's show distinct QW-related features over the entire studied temperature range ($4<T_L<300$ K). In contrast, the low-temperature PMAE spectra of the 50 Å MQW reveal a strong substrate-induced mw absorption at photoexcitation below the (e1:hh1)1*S* exciton band. Figure 4 shows such spectra observed at three temperatures and for $B=0$ and $B=0.09$ T and the corresponding PLE spectra. Comparing them clearly shows that, at low temperatures, the PMA signal is mainly due to free electrons in the GaAs substrate and buffer layer and that the MQW contribution to the PMA signal becomes dominant only for $T_L\geqslant 20$ K. This problem could be overcome by using samples with their substrate removed by chemical etching. Figure 5 shows it by displaying *B*-dependent PMA traces of a 50 Å MQW sample with its substrate removed. They reveal both an electron CR and a hole CR at $T_L=5.5$ K. However, the hole CR is observed at low temperatures only under strong microwave power and high laser intensity.

III. ANALYSIS AND DISCUSSION

In this section we first discuss how the experimental results are used for MQW characterization by comparing the excitation spectra of the photoinduced microwave absorption and of the photoluminescence. Then we analyze the CR lineshape variation with temperature and microwave power in order to learn on electron scattering mechanisms in MQW's and on the effects of weak in-plane localization on the electron and hole cyclotron masses.

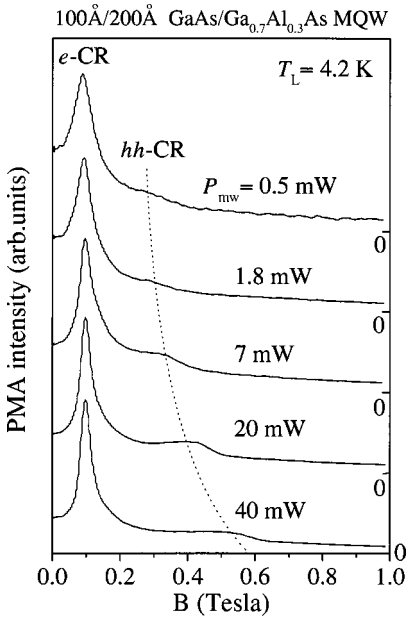

FIG. 3. The magnetic-field dependence of the photoinduced microwave absorption measured in the 100 Å MQW sample for five values of incident mw power at $I_L=100$ mW/cm^2 and $E_L=1.59$ eV. The dotted line is a guide to the eye indicating the hh-CR peak shift with P_{mv}.

A. MQW characterization by comparing microwave absorption and photoluminescence excitation spectra

Electronic characterization of undoped MQW samples is usually done by exciton PL and PLE spectroscopies. The PLE spectrum is closely related (but is not identical) to the absorption spectrum. It is simpler to measure because it does not require GaAs substrate removal.[17] A typical characterization is presented in Fig. 1: The PLE spectrum of the 200 Å MQW shows distinct (e1:hh1)1*S* and (e1:1h1)1*S* exciton bands, and the E_g(e1-hh1) and E_g(e1-1h1) band-gap onsets.

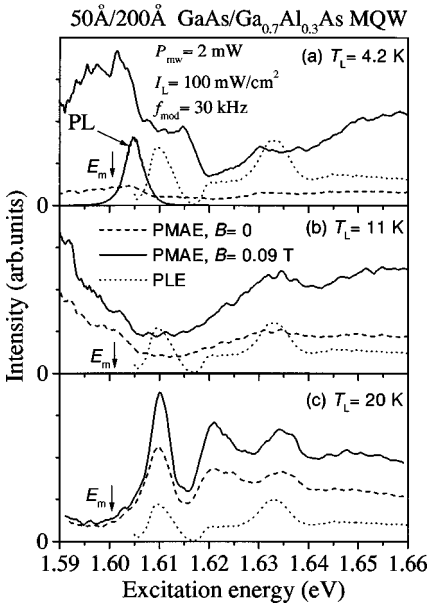

FIG. 4. The PMAE spectra of the 50-Å MQW measured at $B=0$ and $B=0.09$ T, and at three temperatures. The corresponding PLE spectra (monitored at E_m) are also shown for comparison.

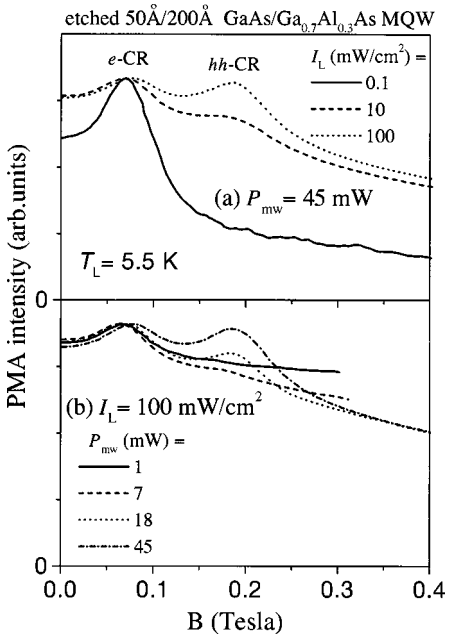

FIG. 5. The magnetic-field dependence of the photoinduced microwave absorption measured at $T_L=5.5$ K, $E_L=1.662$ eV, and $f_{mod}=30$ kHz in a 50 Å MQW sample having its substrate removed. (a) For three different photoexcitation intensities. (b) For four different incident mw power values.

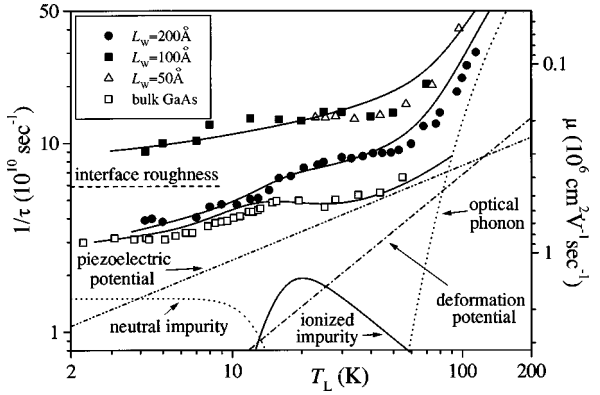

FIG. 6. The temperature dependence of the electron inverse relaxation time and mobility for the three MQW's studied here and for the bulk GaAs sample (the bulk GaAs data were taken from Ref. 7). The values were obtained from CR traces (as in Fig. 2) by using Eq. (1). Also shown are the total model fitting curves obtained using Eq. (3) for the 100 Å and 200 Å MQW's as well as for the bulk GaAs sample (solid lines), and the temperature dependence of each scattering rate given in Table I with parameters corresponding to the 100 Å MQW.

It is well known that as the QW width decreases, the exciton PL and PLE bands broaden and, concurrently, the Stokes shift between their peaks increases. This is due to exciton localization in tail states resulting from potential fluctuations of the interface roughness.[17] In the present case of the 200 Å MQW, the (e1:hh1)1*S* exciton band has the same width in its PL and PLE spectra and no Stokes shift between them. Both PL and PLE spectra show a split (e1:hh1)1*S* exciton band ($\Delta E\sim 0.3$ meV). This is interpreted to be due to excitons moving over large area ''interface islands.'' [17] Thus, we conclude that in the 200 Å-wide MQW, the excitons are essentially free.

We now consider the fact that a PMA signal is observed in the undoped MQW. This means that free carriers are photoexcited alongside the excitons. The PMAE spectrum measures the interband transitions that produce unbound e-h pairs, whereas the PLE spectrum measures those of bound pairs (excitons). As clear (though broader) exciton bands are also observed in the PMAE spectrum, we conclude that excitons dissociate after their photoexcitation. In the following paper[18] we analyze this observation in detail and show that excitons are thermally dissociated at high temperatures and a nonthermal Auger-like exciton dissociation process occurs at low temperatures.[18–20]

We observe that the excitonic features in the low-temperature PMAE spectra are enhanced under high P_{mw} and for a magnetic field value equal to the electron CR field (inset of Fig. 2). The reason is that electron heating by the mw field increases the exciton impact ionization rate,[21] yielding a higher density of unbound electrons and holes.

B. Electron scattering mechanisms and their temperature dependence

The experimental temperature dependence of the electron inverse relaxation time, $\tau^{-1}(T_L)$, extracted from the CR line-shape analysis [by using Eq. (1)], is shown in Fig. 6 for all three studied MQW's. For the 50 Å MQW sample, the τ^{-1} values are shown only for $T_L>20$ K since electron localization in the QW precludes observation of the CR signal at lower T_L. For comparison, also shown is $\tau^{-1}(T_L)$ of a bulk GaAs having the same quality as the QW's (the GaAs buffer layer). The following general observations can be made: (i) At high temperatures ($T_L\geqslant 100$ K), $\tau^{-1}(T_L)$ of all MQW's converge to the same value, determined by polar optical-phonon scattering (see below). (ii) At low temperatures, the MQW's $\tau^{-1}(T_L)$ increases with decreasing L_W and is always higher than that of the bulk sample. This observation is consistent with the theoretical analysis discussed below: in GaAs MQW's, neglecting the interface roughness scattering process, the low-temperature electron-phonon scattering rate is always higher than that of bulk GaAs of the same quality.

The $\tau^{-1}(T_L)$ that is extracted from the electron CR line-shape analysis is identified as the electron momentum relaxation rate. The model used here in order to fit the experimental data assumes that the total momentum relaxation rate is given by the sum of the inverse-relaxation times for each electron scattering mechanism (Matthiessen's rule):

$$\tau^{-1}(T_L)=\Sigma\,\tau_i^{-1}(T_L). \tag{2}$$

This approach has been used to obtain the relative contributions of the main electron scattering mechanisms in many semiconductor bulk materials and in GaAs MQW's at low temperatures.[7,25] These scattering mechanisms are the following: (i) Electron-acoustic phonon scattering via the piezoelectric interaction and deformation potential, and electron-LO phonon scattering via the Fröhlich interaction. (ii) Electron-background impurity scattering, that in QW's refers to in-well impurities. (iii) Electron-remote impurity scattering that is mainly of importance in the case of modulation doped heterostructures. (iv) Electron-interface roughness scattering in the case of QW's.

TABLE I. Summary of electron scattering mechanisms and their rates in two-dimensions.

Type of scattering	Expression for τ^{-1}	Parameters
Polar optical phonons	$\frac{3e^2\hbar\omega_{\rm LO}m^{*1/2}\varepsilon_0^{-1}(\varepsilon_\infty^{-1}-\varepsilon^{-1})}{2^{3/2}\pi^{1/2}\hbar^2(k_BT_{\rm L})^{1/2}(e^{\hbar\omega_{\rm LO}/k_BT_{\rm L}}-1)\chi(T_{\rm L})}$ (from Ref. 25)	$\hbar\omega_{\rm LO}=36.7$ meV (from Ref. 27) $\chi(T_{\rm L})=1$ for $T_{\rm L}<150$ K
Acoustic-phonon deformation potential	$\frac{3E_1^2m^*k_BT_{\rm L}}{2\hbar^3\rho s^2L_{\rm W}}$ (from Ref. 22)	$E_1=7.64$ eV (from Ref. 7)
Acoustic-phonon piezoelectric potential	$\frac{2^{3/2}(m^*k_B)^{1/2}e^2K^2T_{\rm L}}{3\pi^{3/2}\hbar^2\varepsilon\varepsilon_0T_{\rm e}^{1/2}}$ (from Ref. 22)	$K^2=3.59\times10^{-3}$ (from Ref. 7)
Ionized impurities	$\frac{m^*e^4N_i^{(2{\rm D})}}{8\pi(\varepsilon\varepsilon_0)^2\hbar^3}\int_{-\pi}^{\pi}\frac{(1-\cos\Theta)d\Theta}{(q+q_s)^2}$ (from Ref. 2), where $q_s=\frac{m^*e^2}{4\pi\varepsilon\hbar^2}$ (at low tempeatures)	$N_{\rm D}=2.5\times10^{13}$ cm^{-3} (this work)
Neutral impurities	$aN_{\rm N}^{(2{\rm D})}$ (our assumption)	$a=0.75\times10^3$ cm^{2}sec^{-1} (this work)
Interface roughness	$\frac{m^*(\Delta\Lambda)^2}{\hbar^3}\lvert\Gamma\rvert^2\int_0^{\pi}\frac{(1-\cos\theta)e^{-q^2\Lambda^2/4}}{[\varepsilon(q)]^2}d\theta$ (from Ref. 26), where $\Gamma=\frac{\partial E_0}{\partial L_{\rm W}}\cong\frac{\hbar^2\pi^2}{m^*L_{\rm W}^3}$ and $\varepsilon(q)=1+q_s/q$	$\Delta=2.83$ Å $\Lambda\sim25$ Å (this work)

The electron-phonon scattering in bulk semiconductors is governed by momentum conservation, whereas in the 2D case this requirement is relaxed. However, for wide QW's, Price[22] showed that while the electron motion is confined in one direction, the phonons may be considered to be bulklike (disregarding the interface modes). His model calculations indicate that the electron momentum relaxation rate due to acoustic phonons scattering via both the piezoelectric interaction and the deformation potential is enhanced in MQW's as compared with bulk GaAs. On the other hand, the electron momentum relaxation rate due to polar optical phonon scattering in 2D systems is assumed to be the same as in bulk material.[4]

Electron scattering by background impurities is usually neglected in the low-temperature mobility estimates of modulation-doped QW's due to screening. However, we find that this type of scattering is significant in the undoped, high-quality MQW's studied here, as well as in bulk GaAs of the same quality.[7] There is no simple analytic expression for the background ionized-impurity scattering rate in the 2D case.[1,4] We thus use the approach developed in Refs. 1 and 2. The electron scattering by neutral background impurities is taken to be temperature independent, as in the bulk case where this scattering is usually described by the Erginsoy formula.[6]

The temperature-dependent concentrations of the ionized and neutral donors, $N_{\rm i}$ and $N_{\rm N}=N_{\rm D}-N_{\rm i}$, respectively, ($N_{\rm D}$ is the total donor concentration), are estimated as in the bulk case,[7] but using the 2D conduction-band density of states ($\rho_{\rm 2D}=m^*/\pi\hbar^2$):

$$N_{\rm i}=\frac{2N_{\rm D}}{1+\sqrt{1+\frac{8N_{\rm D}}{N_{\rm C}}\exp\left\{\frac{E_{\rm i}}{K_BT_{\rm L}}\right\}}}, \tag{3}$$

where $E_{\rm i}$ is the donor ionization energy and $N_{\rm C}=2k_BT_{\rm L}\rho_{\rm 2D}$ is the 2D effective number of states in the conduction band (for GaAs, $N_{\rm C}=0.48\times10^{10}T_{\rm L}$ cm^{-2}).

The surface roughness scattering process was studied intensively in relation to magnetic field-induced states at the surface of metals[23] and thereafter in Si inversion layers.[1] This subject has been reviewed by Ando *et al.*,[2] who showed that interface roughness scattering is not important in GaAs modulation *n*-doped heterostructures with electrostatic field confinement. This theory was adopted by Sakaki *et al.*[24] to the case of interface roughness scattering due to quantum-well width fluctuations. It was shown that in this case interface roughness scattering is very important (even dominant) and depends on both the height and the lateral extension of the potential fluctuations.

The theoretical expressions for the scattering rate of each process, as well as the parameters used in the data fitting or extracted from it, are summarized in Table I. The following symbols are used: $T_{\rm e}$ – electron temperature, k_B – Boltzmann constant, $\omega_{\rm LO}$ – LO phonon frequency, ε – static dielectric constant, $\varepsilon_{\rm o}$ – permittivity of free space, ε_∞ – optical dielectric constant, K^2 – electromechanical coupling constant, E_1 – deformation potential constant, ρ – crystal density, s – averaged velocity of sound, $q=2k\sin(\theta/2)$ – the magnitude of the 2D transfer wave vector, q_s – screening wave-vector parameter, Δ – interface roughness height, Λ – interface roughness correlation length, Γ – interface scattering strength, and $E_{\rm o}$ – electron confinement energy.

The calculated $\tau^{-1}(T_{\rm L})$ for the 100 Å and the 200 Å MQW's and for bulk GaAs are shown in Fig. 6 by solid lines. (The bulk GaAs calculation is taken from our previous study).[7] Also, the temperature dependencies of each scattering rate τ_i^{-1}, calculated for the 100 Å MQW, are presented

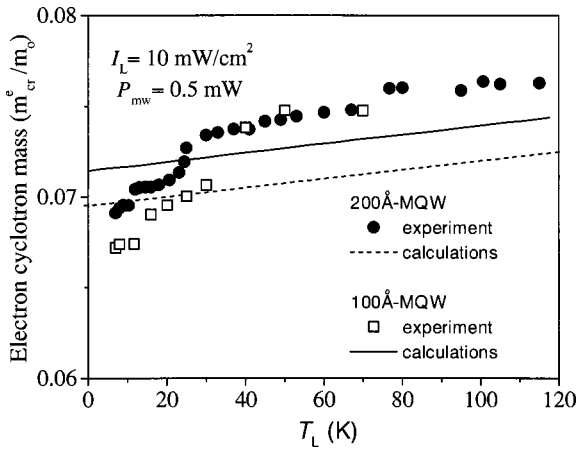

FIG. 7. The temperature dependence of the electron cyclotron mass obtained by fitting the CR traces for 200 Å MQW and 100 Å MQW. The dashed and solid lines are the calculated electron effective mass dependence on temperature for 200 Å MQW and 100 Å MQW, respectively [using Eq. (4)].

separately in Fig. 6. In these calculations, we disregard screening, since the photogenerated electron density is very low. The interaction coefficients for the electron-acoustic phonon scattering (E_1, K^2) were taken from our CR study of bulk GaAs.[7] For the interface roughness potential, namely the ''interface landscape,'' we assume a distribution of ''islands'' with height (along the growth direction) of one monolayer and average size (diameter) of Λ. With $\Delta = 2.83$ Å, the calculated average potential fluctuation is $\delta E = (2E_o/L_W)\Delta$. This gives $\delta E = 0.28$, 1.62, and 7.9 meV for $L_W = 200$, 100, and 50 Å, respectively. These values agree well with the observed (e1:hh1)1S exciton PL linewidths. Thus, in the fitting procedure we used only two free parameters: N_D and Λ (same values for both 200 Å and 100 Å MQW's). A good agreement is obtained between the experimental data and the model calculations with $N_D \sim 2.5\times10^{13}$ cm^{-3} and $\Lambda \sim 25$ Å. This value of volumetric background donor concentration is consistent with that obtained for MBE grown bulk GaAs of the same quality.[7] As for the interface roughness scattering, the value of $\Lambda \sim 25$ Å for the potential fluctuation lateral size is similar to other estimates.[24,28] It indicates that the short-range components of the interface roughness potential are limiting the electron mobility at microwave frequency.

From the fitting procedure, we found that the interface roughness-limited electron mobility is $\sim 1.3\times10^7$ cm^2/Vsec for the 200 Å MQW and $\sim 4\times10^5$ cm^2/Vsec for the 100 Å MQW. Thus, we conclude that in the 200 Å MQW, the low-temperature electron scattering is mainly due to acoustic phonons and background impurities, as in the case of bulk GaAs. On the other hand, in the 100 Å MQW, the low-temperature electron momentum relaxation rate is determined by the interface roughness scattering.

C. Weak localization effect on the electron and hole effective masses

Fitting the CR line shapes by Eq. (1) also yields the carrier cyclotron mass. Figure 7 shows the electron cyclotron mass as a function of temperature for the 100 Å and 200 Å MQW's. In order to compare the experimentally obtained electron effective mass values (m^e_{cr}) with theoretical predictions, we used the following procedure: the in-plane effective mass is calculated by the second derivative of the subband dispersion $E_o(k_\parallel)$ that was calculated using the eight-band model of Baraff and Gershoni.[29] The temperature dependence of the effective mass is obtained assuming that the electron thermal kinetic energy is given by: $\langle E_k \rangle = k_B T_L = E_o(k_\parallel) - E_o(k_\parallel = 0)$. This relation determines a $k_\parallel$ value for a given T_L. In addition to the conduction band nonparabolicity, we take into account the polaron effect that is nearly three times stronger in two-dimensional systems than in the corresponding bulk materials.[30] The estimated mass increase due to the polaron effect is $\sim 1/(1-\pi\alpha/8)$, which is $\sim 3\%$ for the 2D GaAs-based system, where $\alpha \sim 0.07$ is the dimensionless Fröhlich coupling constant for GaAs. Then, the effective mass dependence on temperature, $m^*_e(T_L)$, is given by

$$\frac{1}{m^*_e} = \left(1 - \frac{\pi\alpha}{8}\right)\frac{1}{\hbar^2}\frac{\partial^2\langle E_k\rangle}{\partial k^2_\parallel}. \tag{4}$$

For $T_L > 30$ K, the calculated $m^*_e(T_L)$ increases linearly with approximately the same slope as the experimental m^e_{cr} values do. However, there are discrepancies between the calculated effective mass absolute values and the experimental values (of $\sim 2.5\%$), and the obtained experimental dependence on T_L is steeper than the calculated one, for $T_L < 30$ K. Moreover, in the limit of low temperatures, we observe that the cyclotron mass decreases when L_W decreases, whereas the calculated band-edge in-plane mass values have an inverse dependence. At $T_L = 4.2$ K, the experimental electron cyclotron masses are $0.069m_o$, $0.067m_o$, and $0.055m_o$, and the calculated values are $0.068m_o$, $0.070m_o$, and $0.074m_o$ for the 200 Å, 100 Å, and 50 Å MQW's, respectively. This means that there is another physical mechanism that strongly affects the cyclotron masses at low temperatures. We argue now that it is the weak electron localization at interface islands.

An electron cyclotron mass decrease relative to the band-edge effective mass value has been observed previously by FIR CR in GaAs/$Al_{0.3}Ga_{0.7}As$ quantum structures.[10,31,32] This effect was attributed to weak electron localization at interface islands that arise from long-range potential fluctuations.[33] According to the model described in Refs. 12 and 34, the binding potential in a given interface island is assumed to be described by a harmonic oscillator function of the electron in-plane coordinates. This results in a m^c_{cr} decrease with increasing localization energy.[34] Note that the localization model described in Refs. 12 and 34 requires that the length scale of the potential fluctuations that determine the localization must be larger than the electron cyclotron radius (~ 1000 Å), in order to satisfy the criterion $\omega_c\tau > 1$.

Since the electron localization potential increases with decreasing L_W, we expect the localization effect on m^e_{cr} to be strongest in the 50 Å MQW and negligible in the 200 Å MQW. This is consistent with the observed mass decrease trend mentioned above. Moreover, the temperature dependence of the 50 Å MQW PMAE spectra, shown in Fig. 4, indicates that the QW exciton bands appear only at $T_L \geq 20$ K. We make the simplifying assumption that the av-

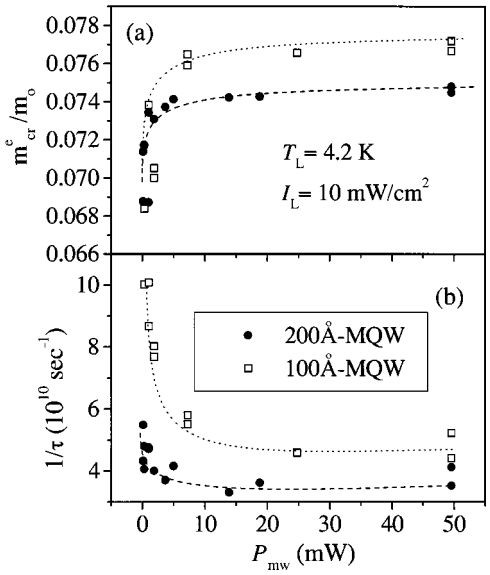

FIG. 8. The mw power dependence of the electron parameters obtained by fitting the CR traces for the 200 Å and 100 Å MQW's: (a) CR masses, (b) inverse momentum relaxation times. The dashed and dotted lines are guides to the eye for the 200 Å and 100 Å MQW's, respectively.

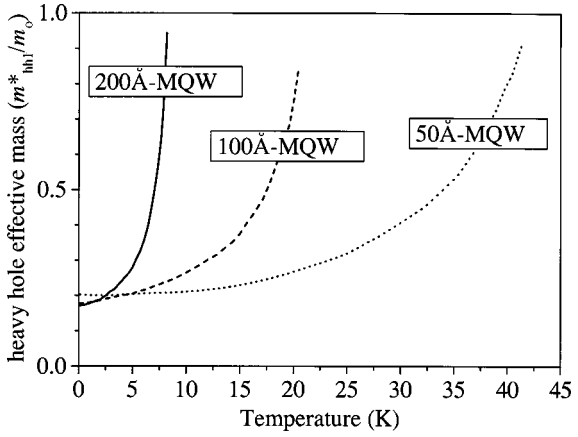

FIG. 9. Calculated temperature dependence of the heavy hole effective masses for the three MQW's [obtained by using Eq. (4)]. The steep heavy hole effective mass increase is due to the hh1 and lh1 band anticrossing.

erage electron localization energy due to the long-range potential fluctuations (that is produced by one monolayer interface fluctuations) is the same $\delta E=(2E_o/L_W)\Delta$ as that of the short-range potential fluctuations. Then, this estimate explains well the observation that at low temperatures ($k_BT_L \sim 0.4$ meV at $T_L \sim 5$ K) the electrons are strongly localized in the 50 Å MQW, but not in the 200 Å MQW, whereas at higher temperatures ($k_BT_L \sim 8.6$ meV at $T_L \sim 100$ K) they are essentially free to move in the QW plane regardless of the QW width.

Increasing P_{mw} (at $T_L=4.2$ K) has a similar effect on m^e_{cr} as that of increasing T_L, but an opposite effect on the scattering rate extracted from the CR traces, as shown in Fig. 8 for the 200 Å and the 100 Å MQW's. The m^e_{cr} increase indicates that the electrons become less localized. τ^{-1} decreases since only the electrons are heated without a concurrent lattice heating, as in ultrapure bulk GaAs.[7] Therefore, the phonon- and ionized-impurity-related scattering processes are less effective under higher P_{mw}. Also, the variations in m^e_{cr} and τ^{-1} are greater in the 100 Å MQW than in the 200 Å MQW. These observations confirm the stronger electron localization in the 100 Å MQW than in the 200 Å MQW, in consistence with the temperature dependence measurements.

The PMA intensity dependence on magnetic field reveals that, in addition to the electron CR band, a second band is observed at a higher magnetic field in the 100 Å MQW and in the (substrate-etched) 50 Å MQW (Figs. 3 and 5). (In the 200 Å MQW, only the electron CR band is observed). This second CR band is weak, relative to the electron CR band in the 100 Å MQW, and its resonance field is very sensitive to P_{mw}, as shown in Fig. 3. In the 50 Å MQW, this second CR band is only moderately shifted with mw power increase. We attribute this additional CR band to the hh CR, based on the following analysis: $m^*_{hh}(T_L)$ is calculated using the same procedure (described above) as for the $m^*_e(T_L)$ calculation. The calculated $m^*_{hh}(T_L)$ is shown in Fig. 9 for all three MQW structures. At $T_L=4.2$ K, the experimentally obtained cyclotron hh masses are $m^{hh}_{cr}=0.21m_o$ for the 100 Å MQW and $m^{hh}_{cr}=0.15m_o$ for the 50 Å MQW. The calculated values are: $m^*_{hh}=0.20m_o$ and $m^*_{hh}=0.19m_o$, respectively. The discrepancy obtained for the 50 Å MQW is attributed to a weak hh localization, according to the same model described above for electron localization.

The calculated $m^*_{hh}(T_L)$ increases very steeply with increasing T_L. This is due to the heavy hole and light hole (lh) subband anticrossing that results in a singularity like variation of the in-plane effective masses for low $k_\parallel$. As L_W increases, the hh1-lh1 subband anticrossing occurs at lower $k_\parallel$, and, consequently, at a lower intrasubband energy (namely, lower T_L). The absence of a hole CR in the 200 Å MQW is thus attributed to an insufficient magnetic field range over the entire experimental temperature range, since the calculated m^*_{hh} singularity occurs already at $T_L \sim 4$–5 K.

In the 100 Å MQW, the hole CR field increases with a P_{mw} increase (Fig. 3), and this is explained by mw-induced hole heating. The hh CR trace is too weak to be reliably fitted by Eq. (1) for a momentum relaxation rate extraction. However, the cyclotron mass can be estimated from the CR magnetic field (the dotted line in Fig. 3 is a guide to the eye for such an estimate). Using the calculated $m^*_{hh}(T_L)$ shown in Fig. 9 and assuming that the effective hole temperature (T_{hh}) increases with P_{mw}, we obtain from the hole CR field that, at $T_L=4.2$ K, T_{hh} increases up to ~ 17 K, for $P_{mw}=40$ mW.

In the (etched) 50 Å MQW sample, the hh CR is observed at low temperatures only under high P_{mw} and high I_L. Note that the P_{mw} increase results only in a small hh CR field shift at $T_L=5.5$ K, as shown in Fig. 5. This result is consistent with the calculations (Fig. 9), wherein the m^*_{hh} value in the 50 Å MQW increases noticeably only for $T_L>20$ K. Concurrent with the hh CR appearance, we observed that the electron CR field increases. Such a shift corresponds to a cyclotron mass variation from $m^e_{cr}=0.055m_o$ to $m^e_{cr}=0.065m_o$. This observation again shows that mw heating activates both electrons and holes out of the shallow spatial potential fluctuations where they are weakly (and separately) localized.

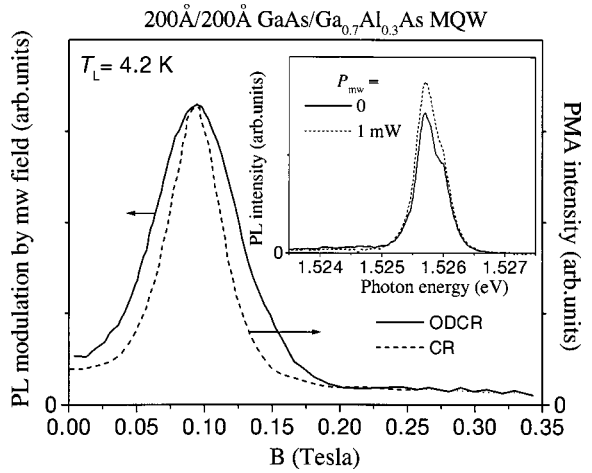

FIG. 10. A comparison between the electron CR and ODCR traces at $I_L=2\,\mathrm{mW/cm^2}$, $E_L=1.54\,\mathrm{eV}$, and $P_{mw}=1\,\mathrm{mW}$. The ODCR trace is monitored at the (e1:hh1) 1*S* exciton band.

IV. CONCLUSIONS

The photoinduced microwave absorption, its excitation spectrum, and the classical electron and hole CR are studied in undoped $GaAs/Al_{0.3}Ga_{0.7}As$MQW's, using combined microwave and optical techniques. The temperature and microwave power dependence of the electron and hole cyclotron masses and their momentum relaxation rates are extracted from the CR line-shape analysis. A detailed analysis of the momentum relaxation rate dependencies is presented for the 100 Å and 200 Å MQW's by adding the rates due to various electron scattering mechanisms. The main conclusions are that in all undoped MQW's, the electron scattering rates are higher than those of bulk GaAs layers of similar crystal quality. In the narrower MQW's, short-range interface roughness scattering dominates over electron-acoustic phonon and electron-impurity scattering.

The PMAE spectra and the cyclotron mass dependence on temperature and mw power are interpreted in terms of weak carrier localization. The analysis suggests that, at low temperatures, the photoexcited electrons and holes in undoped $GaAs/Al_{0.3}Ga_{0.7}As$ MQW's are (separately) localized by long-range, in-plane potential fluctuation arising from monolayer interface fluctuations. The localizing potential strength increases with QW width decrease, but it is sufficiently weak that the localized carriers can be activated into free states by either thermal heating or mw heating (that affects mainly the free carriers).

The hh-mass dependence on well width and on temperature is analyzed in terms of its singularity like dependence on hole energy that results from the hh1-lh1 subband anticrossing.

ACKNOWLEDGMENTS

The work at Technion was done in the Barbara and Norman Seiden Center for Advanced Optoelectronics. It was supported by the Israel Science Foundation (founded by the Israel Academy of Science and Humanities). The authors acknowledge many fruitful discussions with Professor B. M. Ashkinadze.

APPENDIX: OPTICALLY DETECTED CYCLOTRON RESONANCE

When samples consisting of an epilayer grown on a thick GaAs substrate are studied, difficulties arise in obtaining the CR of QW-confined carriers since, under illumination, microwave absorption is photoinduced in the entire sample. Then, ODCR is advantageous since the effect of microwave irradiation is selected by monitoring a specific PL band. However, the ODCR measurements provide only indirect information on the momentum relaxation rates of photogenerated charged carriers since the exciton photoluminescence modulation by the mw radiation is monitored in the ODCR and not the direct carrier PMA.

We compared the CR and ODCR traces of the 200 Å MQW at $T_L=4.2\,\mathrm{K}$ for the same P_{mw} and I_L, as shown in Fig. 10. The ODCR trace was monitored at the (e1:hh1)1*S* exciton band. The electron ODCR is broader than its direct CR, and this shows that the momentum relaxation rate, extracted from the ODCR linewidth, is larger than that deduced from the CR linewidth. The reason is that there is a basic difference between the CR and ODCR methods: ODCR results from the T_e dependence on the magnetic field strength when heating is caused by the microwave irradiation, and from the hot electron effect on the exciton recombination processes. Since the PL intensity is not proportional to the electron temperature T_e,[35,36] the ODCR line-shape analysis of undoped MQW's does not provide a reliable estimate of $\tau^{-1}(T_L)$, and hence of the electron mobility.[7]

*Present address: Gordon McKay Laboratory, Division of Engineering and Applied Sciences, Harvard University, Cambridge, Massachusetts 02138.

[1] F. Stern and W. E. Howard, Phys. Rev. **163**, 816 (1967).
[2] T. Ando, A. B. Flower, and F. Stern, Rev. Mod. Phys. **54**, 437 (1982).
[3] L. Pfeiffer, K. W. West, H. L. Stormer, and K. W. Baldwin, Appl. Phys. Lett. **55**, 1888 (1989).
[4] W. Walukiewicz, H. E. Ruda, J. Lagowski, and H. C. Gatos, Phys. Rev. B **30**, 4571 (1984).
[5] W. Walukiewicz, Phys. Rev. B **31**, 5557 (1985).
[6] E. Otsuka, Jpn. J. Appl. Phys., Part 1 **25**, 303 (1986).
[7] M. Kozhevnikov, B. M. Ashkinadze, E. Cohen, and A. Ron, Phys. Rev. B **52**, 17 165 (1995).
[8] N. Ahmed, I. R. Agool, M. G. Wright, K. Mitchell, A. Koohian, S. J. A. Adams, C. R. Pidgeon, B. C. Cavenett, C. R. Stanley, and A. H. Kean, Semicond. Sci. Technol. **7**, 357 (1992).
[9] J. P. Kotthaus, in *Interfaces, Quantum Wells, and Superlattices, Vol. 179*, edited by C. R. Leavens and R. Taylor (Plenum Press, New York, 1987).
[10] R. J. Nicholas, M. A. Hopkins, D. J. Barnes, M. A. Brummell, H. Sigg, D. Heitmann, K. Ensslin, J. J. Harris, C. T. Foxon, and G. Weimann, Phys. Rev. B **39**, 10 955 (1989).
[11] J. G. Michels, R. J. Warburton, R. J. Nicholas, and C. R. Stanley, Semicond. Sci. Technol. **9**, 198 (1994).
[12] M. Kozhevnikov, E. Cohen, A. Ron, H. Shtrikman, and L. N. Pfeiffer, Phys. Rev. B **56**, 2044 (1997).
[13] K. Seeger, *Semiconductor Physics* (Springer-Verlag, Wien, 1973).

[14] M. Watts, I. Auer, R. J. Nicholas, J. J. Harris, and C. T. Foxon, in *High Magnetic Fields in Semiconductor Physics III*, edited by G. Landwehr (Springer-Verlag, Berlin, 1992), p. 581.
[15] B. E. Cole, J. M. Chamberlain, M. Henini, and T. Cheng, Phys. Rev. B **55**, 2503 (1997).
[16] H. Linke, P. Omling, P. Ramvall, B. K. Meyer, M. Drechsler, and C. Wetzel, J. Appl. Phys. **73**, 7533 (1993).
[17] C. Weisbuch, in *Physics and Applications of Quantum Wells and Superlattices*, Vol. 170 of *NATO Advanced Studies Institute, Series B: Physics*, edited by E. E. Mendez and K. v. Klitzing (Plenum, New York, 1987).
[18] Details are given in the subsequent paper.
[19] A. Hangleiter, Phys. Rev. B **37**, 2594 (1988).
[20] A. C. Ferreira, P. O. Holtz, B. Monemar, M. Sundaram, J. L. Merz, and A. C. Gossard, Appl. Phys. Lett. **65**, 720 (1994).
[21] B. M. Ashkinadze and A. V. Subashiev, Pis'ma Zh. Eksp. Teor. Fiz. **46**, 284 (1987) [JETP Lett. **46**, 357 (1987)].
[22] P. J. Price, Ann. Phys. (N.Y.) **133**, 217 (1981).
[23] R. E. Prange and T. W. Nee, Phys. Rev. **168**, 779 (1968).
[24] H. Sakaki, T. Noda, K. Hirakawa, M. Tanaka, and T. Matsusue, Appl. Phys. Lett. **51**, 1934 (1987).
[25] S. Adachi, *GaAs and Related Materials: Bulk Semiconducting and Superlattice Properties* (World Scientific, Singapore, 1994).
[26] F. Stern, in *Physics and Applications of Quantum Wells and Superlattices, Vol. 170* (Ref. 17).
[27] M. Kozhevnikov, B. M. Ashkinadze, E. Cohen, and A. Ron, J. Lumin. **72–74**, 312 (1997).
[28] A. Gold, Solid State Commun. **60**, 531 (1986).
[29] G. A. Baraff and D. Gershoni, Phys. Rev. B **43**, 4011 (1991).
[30] F. M. Peeters and J. T. Devreese, Phys. Rev. B **31**, 3689 (1985).
[31] R. J. Warburton, J. G. Michels, R. J. Nicholas, J. J. Harris, and C. T. Foxon, Phys. Rev. B **46**, 13 394 (1992).
[32] M. Seck, M. Potemski, S. Huant, P. Wyder, and G. Weimann, Physica B **211**, 470 (1995).
[33] J. P. Kotthaus, G. Abstreiter, and J. F. Koch, Phys. Rev. Lett. **34**, 151 (1975).
[34] H. J. Mikeska and H. Schmidt, Z. Phys. B **20**, 43 (1975).
[35] B. M. Ashkinadze, V. V. Bel'kov, and A. G. Krasinskaya, Fiz. Tekh. Poluprovodn **24**, 883 (1990) [Sov. Phys. Semicond. **24**, 555 (1990)].
[36] E. Hanamura and T. Inui, J. Phys. Soc. Jpn. **17**, 666 (1962).